Composites Science and Technology 264 (2025) 111123

Contents lists available at ScienceDirect

Composites Science and Technology

journal homepage: www.elsevier.com/locate/compscitech

Comparative analysis of NOL-ring tensile strength in towpreg and slit-tape for filament winding: Influence of resin viscosity, tack, and consolidation

Eduardo Szpoganicz [a], Fabian Hübner [b], Marius Luik [a], Jeremias Thomas [a], Florian Max [a], Andreas Scherer [c], Tobias Dickhut [c], Holger Ruckdäschel [a,*]

[a] Department of Polymer Engineering, University of Bayreuth, Bayreuth, Germany
[b] Airbus Central Research and Technology, Munich, Germany
[c] Department of Aeronautical Engineering, Bundeswehr University Munich, Munich, Germany

ARTICLE INFO

Keywords:
NOL-Rings
Filament winding
Carbon-fiber
Towpregs
Slit-tapes
Cryogenics

ABSTRACT

This study investigates the tensile strength of carbon-fiber reinforced polymer (CFRP) specimens manufactured via filament winding with varying winding parameters. NOL-rings (Naval Ordnance Laboratories) were processed using unidirectional CFRP material, and the performance of towpregs was compared to slit-tapes of different widths and temperature settings. To establish a benchmark, autoclave-cured prepregs were laminated into flat rectangular samples. The manufacturing process revealed significant variations in laminate strength and ply consolidation, analyzed through optical micrographs and profile analysis. Tensile strengths of the NOL-rings ranged from 1430 MPa to 1800 MPa, with towpregs performing better due to higher tackiness and improved consolidation, compared to slit-tapes with no applied temperature. However, both were still bellow the 2100 MPa strength of autoclave-cured reference samples. Finite element analysis showed that the NOL-ring geometry induces bending stresses, even in an idealized part, reducing the theoretical tensile strength to 1900 MPa. Additionally, in-situ cryogenic testing using liquid nitrogen was reported for the first time for NOL-ring specimens, revealed a significant increase in strength to 2200 MPa, attributed to the stiffening effect at low temperatures. This work introduces a novel approach by correlating ply consolidation with slit-tapes, towpregs, and winding parameters, linking prepreg tackiness to tensile performance, and presenting additionally testing of NOL-rings at 77 K, thus providing understanding of their behavior in cryogenic environments.

1. Introduction

Utilizing hydrogen as an energy carrier derived from renewable sources holds significant promise for shaping the future of the mobility and aviation sector, heading towards reduced emission technologies [1–5]. Hydrogen can be stored as gas (high pressure, 700 bar) at room temperature (RT) or as liquid (low pressure, 5–8 bar) at cryogenic temperatures (CT) [1]. When hydrogen is used in a fuel-cell to provide mobility in a vehicle, a storage system is necessary. Recently, composite vessels for hydrogen storage have gathered increasing interest in industry sectors like automotive [6,7], transportation [8,9], aviation [10,11], and space [12–15]. While gaseous storage (Type IV) is more appealing to the mass market (such as automotive and transport), cryogenic liquid storage (Type V) is furthermore relevant for aviation and aerospace due to a much higher energy density [3]. The major difference between both is the use of CFRP composites. Type IV is used in all-composite structures, as a polymeric linear fully wrapped in CFRPs. Whereas the CFRP composite provides strength to the high pressures while in service, the tightness is maintained by the liner made from low permeable polymers, such as polyethylene or polyamide [16,17]. In cryogenic, the walls can be much thinner because the pressures are substantially lower, yet they must withstand the cryogenic temperature condition of the liquid hydrogen (LH2) at −253 °C [18]. Due to the expressive dimension variation when swinging from RT to CT and back to RT, a liner is herein unfeasible. This means, only the composite must maintain the tightness and strength in Type V vessels. As a result, the manufacturing route, quality, and related material selection are of utmost importance for the different scenarios. These rotational symmetric storage vessels are usually manufactured via filament winding process [19,20].

In the conventional filament wet winding, dry fibers are pulled through a liquid epoxy resin bath, impregnated *in-situ*, and wound on a

* Corresponding author.
E-mail address: holger.ruckdaeschel@uni-bayreuth.de (H. Ruckdäschel).

https://doi.org/10.1016/j.compscitech.2025.111123
Received 31 January 2025; Received in revised form 19 February 2025; Accepted 21 February 2025
Available online 22 February 2025

mandrel. This leads often to local variation in fiber volume content, resin-rich areas and limited spreading and impregnation behavior of the tows. All of this leads to rather poor mechanical performance yet to a feasible cost/performance ratio for a potential mass market [19]. In contrast, towpregs are more advanced in terms of quality. They are pre-impregnated externally through a calendaring force with a more medium viscous and honey-like resin. The material exhibits reduced flow, enabling faster processing and minimizing splashing phenomena during production. Nevertheless, the towpregs showed a rather high cured ply thickness (125–250 μm) and exhibit a non-homogeneous distribution of fiber and resin. This leads to a limited quality with a stronger variation of the width but with an intermediate price-performance ratio [21]. Experimental studies of tow-spreading techniques and their benefits towards filament winding were shown in detail by S. Sihn et al. [22]. The highest performance of composites can be derived from slit-tapes. Here, a whole calendared prepreg with precise fiber volume content (often aimed at 60 vol%) was used. Wide tapes of ¼″ or ½″ were cut with precision according to aerospace standards in width variation (<1 % tolerance) which drives the highest laminate qualities and lower ply thickness. The aforementioned prepreg process with additional slitting and rewinding of the tapes results in very high pricing, mostly not suitable for a cost sensitive mass market production [23,24].

Typically, towpreg winding is associated with wet-filament winding, although their origins arise from variations in resin performance due to differences in viscosity. Slit-tapes, while exhibiting exceptional stability and thus performance in laminates, tend to be relatively costly and less readily available for the vessel market. All evaluations involve both merits and drawbacks in terms of quality, price-performance, and material throughput for each of their respective processing routes. Moreover, products are typically designed and engineered based on laminate specifications and often rely on non-representative coupon measurements, which may experience significant deviations due to the manufacturing process. The process can use safety factors to reduce the theoretical material performance, ensuring it accounts for real-world uncertainties and improves reliability. Regarding wet-wound materials, there is often a dearth of coupon comparability due to the presence of liquid resin, which can typically not be accommodated in the prepreg route. Instead, it is processed with stitched fabrics in infusion, a process that notably alters the overall behavior. Flat plates are commonly wound nowadays, making them more comparable to flat layup laminates, though issues with tension distribution are still present. Since the hydrogen vessels mentioned here are also wound, it is significant to consider the winding process, as it directly affects the quality and strength of the resulting laminate.

In this study, split-disk NOL-rings (Naval Ordnance Laboratories) were wound using a reference CFRP system, with varying processing parameters for towpregs and slit-tapes. The wound systems were compared to ideally autoclave-cured coupon laminates with identical cured ply and laminate thickness. Notably, a comprehensive comparison of slit-tapes, towpregs, and wound parts is currently lacking in the literature, which this study addresses. The hot-melt epoxy resin was intentionally chosen to ensure stability in the properties of the laminates. Another novel point of this study is the detailed evaluation of prepreg tackiness between these two material types (slit-tapes and towpregs), which has not been highlighted in previous research. Laminate consolidation was assessed using microscopy and profilometer analysis to understand its impact on mechanical properties. The effect of different parameters used for the NOL-ring systems manufacturing on consolidation was evaluated through the performance at tensile testing, first at RT. Finite Element (FE) analysis was also used to provide further insights into the effect of NOL geometry on the mechanical performance of the wound systems. Furthermore, an innovative adaptation of the NOL-ring tensile testing setup was developed for cryogenic testing, where tests were performed *in-situ* with liquid nitrogen (LN2) to replicate conditions of cryogenic storage tanks.

2. Materials and methods

2.1. Materials

For this study, aerospace-grade unidirectional carbon-fiber of HexTow® IM7 from Hexcel Corporation (Stamford, USA) and a modified epoxy resin were combined to formulate the prepreg composite material. The resin herein was specifically aimed for thin-plies and filament winding of type V composite pressure vessels. **Genioperl W36®** (Wacker AG, Burghausen, Germany) was added at 5 vol% to 100 parts of the matrix mixture. This siloxane-containing block-copolymeric toughener forms **micelle-like core-shell structures** within nanometer-sized domains, optimizing overall toughness. For further details on the utilized epoxy resin, refer to Ref. [20]. Seeking to enhance the consolidation of the filament-wound prepreg plies, a polyester shrinkage tape, R220® from Dunstone (Charlotte, USA), was placed over the surface of the laid up laminates.

2.2. NOL-ring manufacturing

Testing NOL-ring specimens for wound parts is interesting because it allows for the evaluation of the effects of specimen geometry and curvature on the mechanical performance of the according CFRP material. The prepreg material used as slit-tapes was impregnated using a hot-melt prepreg unit from Roth Composite Machinery GmbH (Steffenberg, Germany). A representation of the manufacturing process for both slit-tapes and towpregs is shown in Fig. 1, intended for the fabrication of NOL-ring specimens.

At the top of Fig. 1, a thin-ply prepreg tape with a weight of 70 g/m^2 was produced and then slit into tapes of ¼″ and ½″ width by Omega Systèmes (Nantes, France). The winding machine used for preparing the towpreg material and NOL-ring samples was a 2-axis tabletop winder from Engineering Technology Corporation (Salt Lake City, USA). The rotational speed was set at 40 rpm on a split-disk tool with a diameter of 144.5 mm, resulting in an absolute winding speed of 18.2 m/min [25]. Photographs illustrating the lab-scale wet-winding and towpreg manufacturing process are shown at the bottom of Fig. 1. Finally, both slit-tapes and towpreg materials were wound in hoop layers to produce the NOL-ring specimens.

Samples were cured in a convection oven at 110 °C for 2 h (precuring and gelation) followed by 135 °C (post-curing) to achieve >99 % conversion, with a cool-down rate of 1 K/min to minimize thermal stress. Prepreg materials (towpreg or slit-tape) were passed through rollers at controlled tension (8–10 N, measured via a tension gauge). Resin viscosity was adjusted by heating (50 °C) during winding, influenced by winding speed and contact angle. For NOL-ring manufacturing, the contact angle was 0° and the winding speed was 40 rpm. Parameters for each system are detailed in Table 1. Target fiber volume content (FVC) was 58 ± 2 %, with a cured thickness of ~1 mm from 14 layers (approx. 70 μm per layer). A reference group of tensile bars was prepared with 200 mm prepreg tape via autoclave and tested according to ASTM 3039, while NOL-rings were manufactured following ASTM D2290. Slit-tapes of ½″ and ¼″ were brought to this study to evaluate the effects of drilling end-notch at the specimen edges, as both the curvature and cutting process can create significant stress concentrations.

2.3. Optical microscopy & profilometer

The cured laminate and NOL-rings specimens were analyzed without polishing, with the exclusive purpose of evaluating the consolidation of the layers. Herein, an automated microscope with a high-resolution Leica DFC450 digital camera (Wetzlar, Germany) was utilized. Preliminary work established a magnification of×100 and × 200 for evaluation of the laminate consolidation. Every specimen herein was analyzed. The profile analysis via white-light interferometry was conducted using the Keyence vr-5000 Profilometer (Neu-Isenburg,

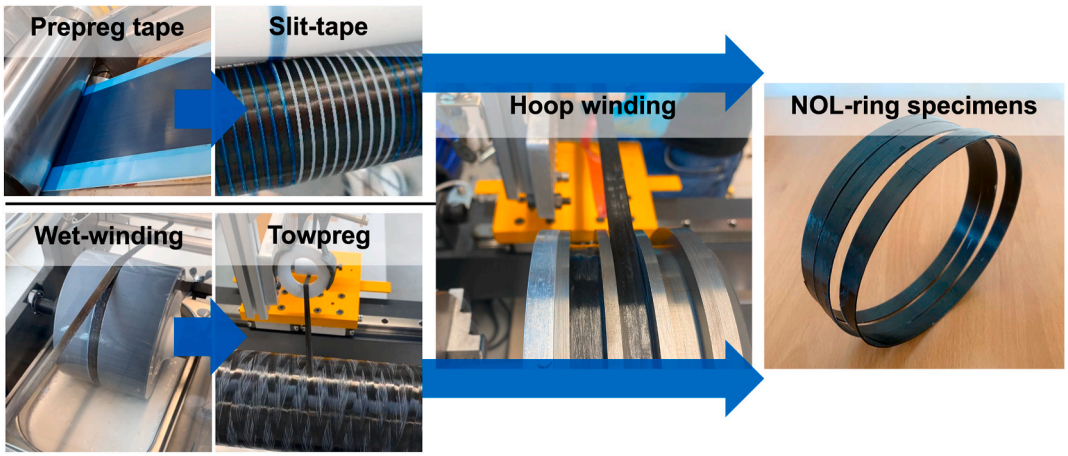

Fig. 1. Schematic images of the thin-ply prepreg tape manufacturing and as slit-tape (top), the wet-winding and towpregs lab-scale manufacturing process (bottom), followed by hoop winding and NOL-ring specimen manufacturing.

Table 1
Summary of prepared systems for testing survey and their information.

Sample	Winding temperature	Curing process	External compaction	FVC	Average thickness
Reference *Rectangular laminate 0°*	–	Autoclave	4 bars	59 ± 2 %	0.98 ± 0.08 mm
NOL1 *½″ slit-tape*	RT	Oven	–	58 ± 2 %	1.16 ± 0.10 mm
NOL2 *¼″ slit-tape*	RT	Oven	–	58 ± 2 %	1.17 ± 0.09 mm
NOL3 *¼″ slit-tape + R220®*	RT	Oven	[a]0.6 bar	58 ± 2 %	1.07 ± 0.06 mm
NOL4 *¼″ slit-tape + R220® + heated mold*	50 °C	Oven	[a]0.6 bar	58 ± 2 %	1.10 ± 0.04 mm
NOL5 *¼″ towpreg*[b]	50 °C	Oven	–	57 ± 3 %	1.18 ± 0.09 mm

[a] The 0.6 bar pressure herein is estimated based on the R220® product datasheet.
[b] The ply-thickness of the towpreg is 140 μm, compared to the 70 μm of the slit-tapes.

Germany). The images were taken with × 80 magnification. The profile was measured using the high-resolution settings.

2.4. Tack measurements and shear rheology

Tack measurements of the prepreg material (either as slit-tape or towpreg) was carried out. The tackiness of the prepreg was assessed using a Zwick Z050 universal testing machine (Ulm, Germany), fitted with a 200 N load cell. The probe tack test setups were modified in accordance with ASTM D2979. The adapted setup of this measurement is described more in detail by Ref. [26]. Here, a contact force of 30 N was applied, during a contact time of 5 s. The debonding rate was set as 30 mm/min. To obtain insight into the effect of the material process and consolidation, three different conditions were given to the prepreg materials to represent the systems mentioned in Table 1, shown in Table 2. Notice that the reference system cannot be herein compared, as its compatibility relies solely on the autoclave process.

The rheology of the resin utilized for this work was also investigated to better understand the leading parameters and correlations between prepreg tack and consolidation. The data obtained for the shear-rheology temperature sweep experiment was measured through a rotational rheometer Anton Paar MCR 301 (Granz, Austria). The complex viscosity of the resin was evaluated as a function of the temperature.

Table 2
Schematic correlation between NOL-ring system and measured tackiness.

Tack Specimen	Temperature	→	Representative system
Slit-tape	RT	→	NOL1, NOL2 & NOL3
Slit-tape	50 °C	→	NOL4
Towpreg	50 °C	→	NOL5

2.5. Tensile testing

The tensile testing of all mentioned systems was carried out according to standards ASTM 3039 (Reference) and ASTM D2290 (NOL-rings). Six to eight specimens were tested in a universal testing machine (ZwickRoell GmbH & Co. KG, Germany), equipped with a load cell of 250 kN. For the reference tensile bars specimens, a standard clamping system setup was used with clamping pressure of 50 bars. For NOL-ring specimens, the supports are designed as half-disks shown in Fig. 2. The supports for holding the tension test fixture are self-aligning. Standard testing environment conditions were maintained as RT and relative humidity of 50 %. The crosshead speed was given as 2 mm/min. An axial strain gauge sensor was attached to the surface of the samples, on an attempt to properly determine the Young's modulus and the strain at failure.

For testing at CT, an identical testing setup was employed, supplemented by a metallic dewar. A vacuum gap double wall construction is included herein so the LN2 is stable throughout the test. This setup ensures that the specimen is consistently tested at 77 K. Fig. 3 illustrates the detailed testing setup (left) and captures the *in-situ* testing in progress (right).

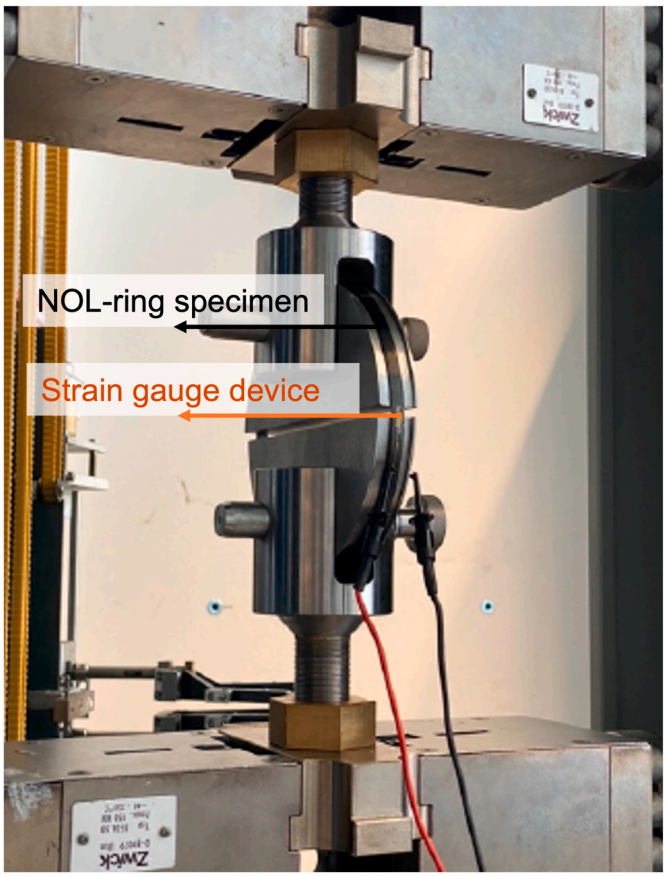

Fig. 2. Schematic NOL-ring tensile testing setup at RT with a strain gauge device.

3. Results and discussion

3.1. Optical microscopy

Microscopy images of the reference flat laminate and the NOL rings were taken from a lateral-longitudinal view, to compare the consolidation quality within the layers and the overall level of delamination in the specimen. The optical micrographs in Fig. 4a reveal a significant variation in consolidation regularity from the autoclave-cured specimen and the NOL-ring systems without *in-situ* external heat source. The high-viscosity resin, which provides ideal conditions for thin-ply prepreg manufacturing and slitting for slit-tapes, can make it difficult to homogenize the layers during the process.

The images in Fig. 4a show an fine case of layer consolidation of a CFRP laminate. The layers here are regular and homogeneous throughout the thickness, and do not show indicators of delamination on a macroscopic level. The images in Fig. 4b and c show the consolidation of ½″ (NOL1) and ¼″ slit-tape (NOL2) specimens, respectively, without any source of heating or external compaction. Notice here the irregularity, with numerous shaped voids and pores scattered throughout the layers. They appear as dark-shaped regions in the image. Intuitively, the use of winding force alone is not enough to place and consolidate the layers homogeneously.

The incorporation of an external source of pressure during the curing process, i.e. using the shrinkage tape in NOL3, seems to have a slight but significant effect, as shown in Fig. 4d. The compaction force of the polyester tape can reach as high as 40 Psi (2.7 bars), depending on the parameters of overlapping, tension, and wound radius. The external pressure during cure here was estimated in 0.6 bars, based on the product datasheet. The enhancement of the layers consolidation here is still apprehensive, but it seems that delamination and shaped porous are more local rather than throughout the specimen thickness. Finally, the optical micrographs of NOL4 and NOL5 are shown in Fig. 4e and f. Here, a consolidation quality comparable to the autoclave-cured composite is seen (compared to Fig. 4a). The resin viscosity seems to take a major role in consolidation, and it is therefore critical that it is found on a specific range during the filament winding process. The images reveal no significant delamination like in previous cases, except for very few irregular spots. Towpregs and slit-tapes show optimum consolidation of the layers by heating the mold at 50 °C.

3.2. Profilometer

Using a profilometer to evaluate the wound product provides a detailed view of the material's surface, allowing detection of porosity and features like under-compacted spots. Fig. 5 shows the profiles of NOL-rings and the reference. In Fig. 5a, the reference autoclave laminate sample is shown, where no defects or disconnected layers are found. Only minor surface variations are detected. In contrast, Fig. 5b reveals severe defects between the layers of the NOL1 system, indicating more than just surface roughness, e.g. delamination between plies. Fig. 5c and d show the NOL4 and NOL5 systems, respectively. These images are very similar to the laminate reference in Fig. 5a. Like the comparison in Fig. 5, the NOL4 and NOL5 systems appear properly compacted, with only minor roughness spots and darker stripes between the plies. Towpregs usually contain more local resin deviation than slit-tapes, and their processing can lead to variations in tape thickness, resulting in noticeable roughness. However, despite the differences in resin viscosity and tackiness affecting consolidation quality, no critical spots are detected here. Notice that the NOL2 and NOL3 specimens exhibited images very similar to those of NOL1 and were thus omitted from Fig. 5.

Fig. 3. Schematic NOL-ring tensile *in-situ* testing setup with LN2.

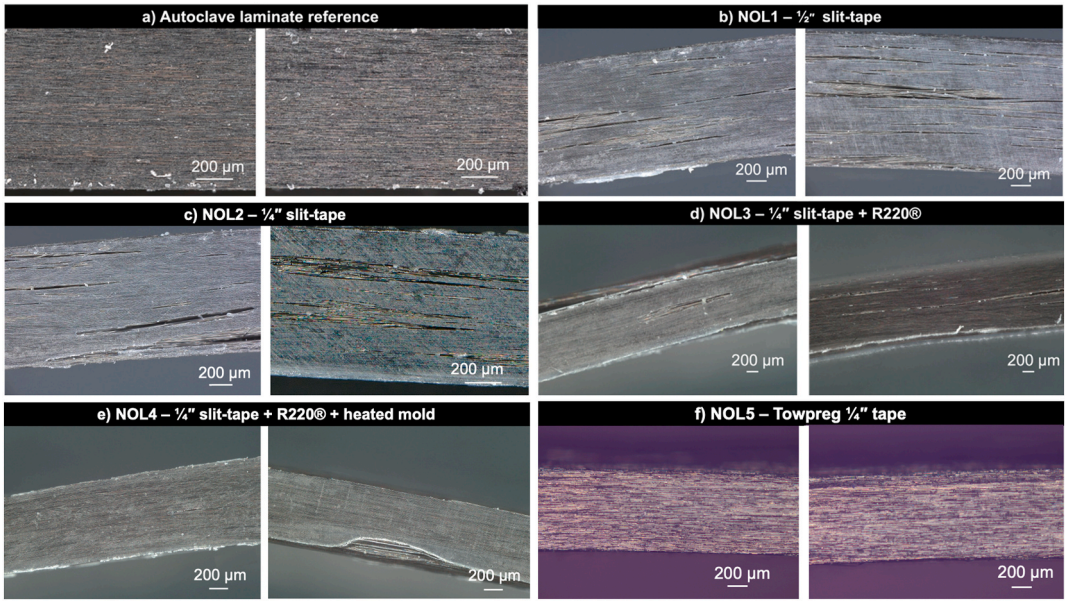

Fig. 4. Microscopic images of a representative specimen in the lateral-longitudinal cut direction for consolidation analysis as a) autoclave laminate reference, b) NOL1, c) NOL2, d) NOL3, e) NOL4, f) NOL5.

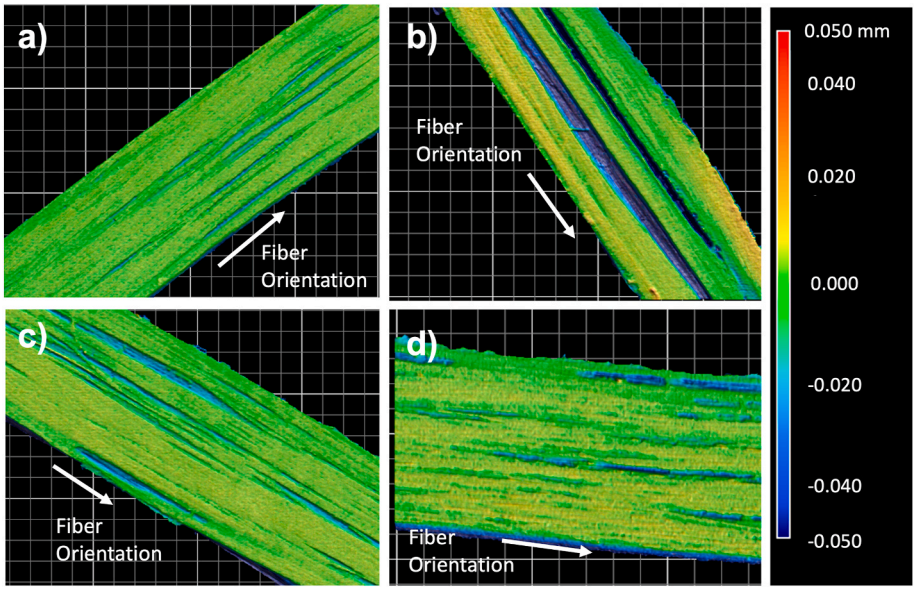

Fig. 5. Profile images of a representative specimen in the lateral-longitudinal view for consolidation analysis as a) autoclave flat laminate reference, b) NOL1, c) NOL4, d) NOL5.

3.3. Resin viscosity and prepreg tackiness

The tackiness of slit-tape prepreg and towpregs was measured at RT, 50 °C, and 80 °C, with 50 °C identified as optimal for maximizing tackiness due to resin viscosity within 10^4–10^6 mPa s (Fig. 6). Towpregs showed higher levels of tackiness than slit-tapes, attributed to their higher resin areal weight (65 gsm vs. 35 gsm, respectively) and ply thickness (140 µm vs. 70 µm, respectively). This could eliminate the need for external pressure. However, for slit-tapes, the overall lower resin areal weight and tackiness imply the need for external pressure to achieve optimal consolidation. This difference is likely to be minimized when the towpregs and slit-tapes have the same resin areal weight and ply thickness.

Resin viscosity within 10^4–10^6 mPa s optimized prepreg tack force, whereas high-viscosity resin at RT limited resin flow, reducing adhesion and tack force. As temperature rises, the resin viscosity decreases, and flow is encountered within the tack stamp. Thus, the resin balances out flowability maintaining stiffness enough to generate a coherence force. This is usually the temperature-viscosity spot where prepreg tack is maximal, and thus where winding manufacturing should target to maximize consolidation. Lastly, when the temperature is risen to 80 °C, the prepreg is still significantly tacky. However, the resin's modulus already degrades to a certain level. Consequently, the values of prepreg tackiness are decreased.

When correlating with prepreg tack, the resin viscosity at RT is 10^8–10^9 mPa s proves non-optimal for tack and adherence, explaining why NOL-rings cannot be properly consolidated at this temperature. As the temperature increases and viscosity drops to 10^5–10^6 mPa s, prepreg tackiness becomes optimal, ideal for consolidating the material into a laminate before curing. However, at 80 °C, the resin's stiffness degrades

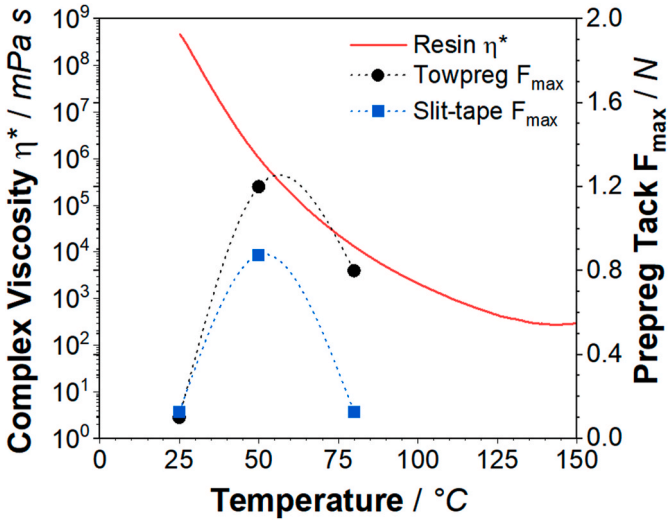

Fig. 6. Resin complex viscosity (left axis) and respectively prepreg tackiness (right axis) as a function of the temperature for the neat resin, towpregs and slit-tapes.

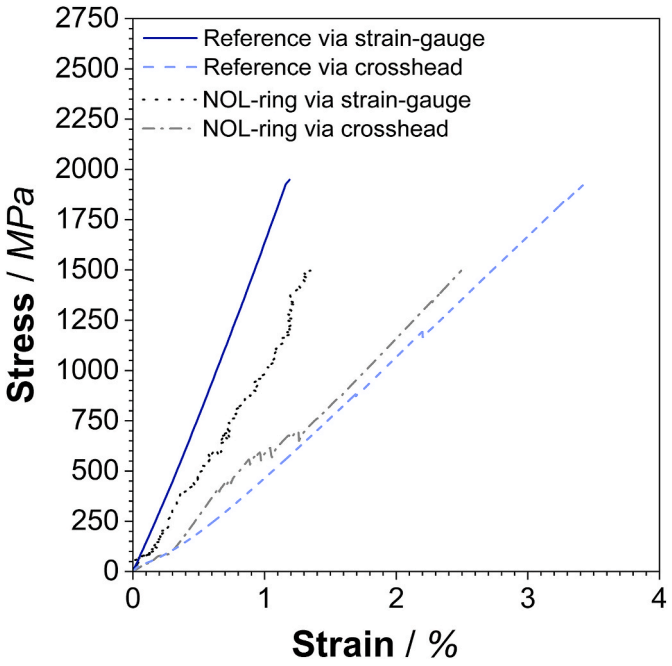

Fig. 7. Tensile stress-strain measurements of the reference laminate material and NOL-ring specimens (NOL2) analyzed via crosshead displacement and with strain-gauge.

significantly, preventing proper adhesion strength to the stamp and thus decreasing the overall tackiness.

3.4. Tensile strength at room temperature

The feasibility of attaching a strain-gauge device to the composite NOL-rings was evaluated by comparing the stress-strain curve from the local sensor and crosshead displacement. The reference laminate was compared with the NOL2 system, shown in Fig. 7. Results showed a degraded signal for NOL-rings, likely due to partial compression on the curved surface during tensile measurements, while flat tensile bars provided clear signals. Despite the noisy signal and strain uncertainty on NOL-rings, the absolute strain failure values were comparable.

Determining strain failure and Young's modulus via traverse displacement is inaccurate here, as the curves show a clear displacement of the signal, caused by the displacement of the tool itself. In view of high forces required to perform the test, values of strain at failure and Young's modulus for NOL-ring specimens were unable to be determined via crosshead displacement. Similar works in literature testing NOL-rings also discuss the difficulty of obtaining the Young's modulus in this case [27,28]. The strength of the NOL-rings is, on the other hand, independent from the strain signal and can be therefore measured with precision.

Considering the similar mode of failure between the two different samples, it is expected a similar range of strain failure, even when the NOL-rings contain a pre-level of strain due to the winding angle. In Fig. 8, a view of the failed specimens clearly shows the strong dissipation of energy via the ductile matrix, leading to a longitudinal splitting. This indicates that the fibers remain mostly intact while the matrix collapses, dividing the specimens into narrower rings until they can no longer withstand the load.

To evaluate the effect of layup and consolidation quality, the ultimate failure of all NOL-ring systems was compared to the ultimate failure of the reference tensile bar. The values are shown as bar charts in Fig. 9. The tensile strength of the unidirectional 0° CFRP laminate (Reference) was evaluated in average 2043 MPa. A significant impact on the laminate strength is seen simply by switching from tensile bars to NOL-ring specimen. A likely reason for this is the bending effect when testing, as the tested segment is no longer a flat bar, but a segment of a circumference (see **Session 3.5**) where the simulation analysis reveals the significant bending effect caused solely by the geometry of the specimen). Considering this geometric effect, it could be assumed that a pre-stress level is already ongoing within the specimen. Therefore, a NOL-ring specimen is unlikely to achieve the same tensile strength performance as a rectangular flat laminate.

The NOL-ring systems 1 and 2, manufactured with the slit-tape without heat nor external compaction force, exhibited the lowest results. Associated with Fig. 4b and c, the layup quality of these systems was low, showing multiple spots of delamination and irregularity within their consolidation. Such delamination spots will certainly lead the delamination mechanics towards early failure, reaching a maximum average stress of 1430 MPa for system NOL1, and 1570 MPa for system NOL2. In between these two systems, the system NOL1 (½″ slit-tape) is additionally drilled with a reduced section (see ASTM D2290), which suggests being as aggressive as low-quality consolidation, given the further decrease in value. The images taken from the profilometer in Fig. 5 show delaminated spots which will initiate the damage process, leading the material to early failure. As mentioned in Section 3.3, the low prepreg tackiness at RT disables good adherence between plies, resulting in these poor-quality laminates.

The use of shrinkage tape alone to manufacture the NOL-rings showed improvement in the consolidation quality, as seen in Fig. 4d. The subsequent effect on the tensile properties of the NOL-rings, however, was still apprehensive. Although the occurrence of voids and delamination has decreased from widespread to localized regions, these areas are still believed to have a significant influence on the specimen performance. The ultimate failure of system NOL3 rises to 1703 MPa, still showing a large deviation from the reference tensile bars. As the tackiness of the slit-tapes herein is kept, the consolidation quality of the final CFRP product is inadequate.

The systems NOL4 and NOL5, which showed layup quality comparable to autoclave tensile bars, were evaluated at the highest strength levels among the NOL-ring systems. NOL4 had an average strength of 1790 MPa, while NOL5 reached 1828 MPa. The strength increase observed for NOL4 and NOL5, relative to NOL1, NOL2, and NOL3, is supported by the micrographs shown in Fig. 4 and the profile in Fig. 5. The results indicate that resin viscosity plays a more significant role ultimately for the layup quality.

The higher tackiness observed for slit-tape and towpregs at 80 °C suggests that maintaining high tackiness during winding is essential for

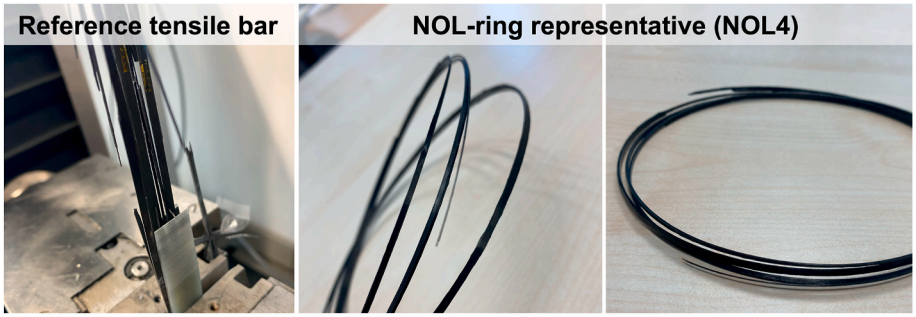

Fig. 8. Visual analysis of reference tensile bar and NOL-ring specimens tensile tested longitudinal to the carbon-fibers at RT.

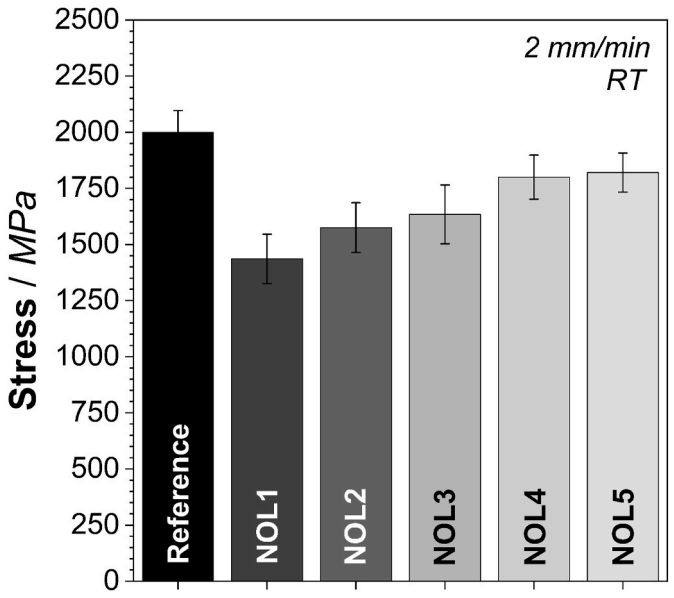

Fig. 9. Ultimate failure stress of NOL-ring systems and reference tensile testing at RT.

achieving optimal consolidation. Additionally, allowing friction along the pattern (not just along the geodesic path) enables more complex winding paths, potentially improving structural adaptability and performance. This becomes even more important when winding angles are involved, as the tapes are pulled in specific directions. However, the strength values for NOL4 and NOL5 are still lower than the reference system. Wound parts with complex shapes or sharp edges, like NOL-rings, can develop localized stress concentrations, weakening the structure. This is especially noticeable when fibers deviate from their natural alignment. Moreover, applying tensile force to flatten the specimen generates indirect bending stress, which reduces the composite's tensile strength. These can be again related with the findings of finite element anylsis in Section 3.5.

3.5. Finite element analysis for room temperature testing

Finite element (FE) analyses were performed based on the as-built geometry of the tested NOL-ring specimens to conduct virtual testing. These simulations were carried out to provide indicators of the bending effect caused by the curvature of the NOL-ring specimens, ensuring alignment with the experimental tests discussed in Section 3.4. The results offer a view of the significant factor contributing to the strength reduction of the NOL-ring specimens compared to the reference laminate. The specimen geometry followed ASTM D2290, except for the NOL1 design, which omitted the drill cuts for area reduction. The simulation was implemented with Abaqus/CAE 2021 software, with a mesh consisting of approx. 22000 nodes to model the whole setup. Preliminary simulations have been conducted to determine the optimal mesh size.

The simulation part consists of three structural components: the NOL-ring, the grips (upper and lower) and the bolts. The boundary conditions of the mathematical model represent those of the physical test where the lower grip will remain fixed in all directions, while the upper grip will be fixed in all directions except the longitudinal direction, where it will be free to move in upward direction as the load is applied. A second cylindrical coordinate system is used as base system for the definition of the layup orientation of the composite layers. Between the NOL-ring and the grips a general contact definition is established considering a hard contact formulation for normal behavior and a penalty friction with a coefficient of 0.25 for tangential behavior. Relevant material properties applied herein are shown in Table 3.

Fig. 10a shows the FE mesh of the NOL-ring testing setup. Preliminary analyses were already performed for mesh convergence studies. The tensile stress failure is derived at approximately 1900 MPa, as shown in the perspective of Fig. 10b. A uniform deformation factor of 10 is displayed. Furthermore, an approximated image of the lateral section of the NOL-ring specimen under load, resulting in a bending effect due to the geometry, is seen in Fig. 10c. These analyses aim to provide deeper insights into the effect of wound geometries under tensile stress, with further developments expected to refine and expand the modeling approach.

The FE analysis aligns with the experimental results, showing that NOL-ring specimens inherently perform worse than flat tensile specimens. The simulation predicts an ideal tensile strength of 1900 MPa for the NOL-ring specimen, while the experimental value for the reference tensile bar is 2043 MPa. This difference can primarily be attributed to the bending moment at the end of the tool, where the free length of the sample is located, due to its curvature. The FE model assumes an idealized specimen, free from defects and unconsolidated areas. This suggests that the reduction in strength is mainly caused by the bending effect from the NOL-ring's curvature, rather than by issues with laminate consolidation.

The simulation in this study was used primarily to explore the effect of the NOL-ring geometry on strength reduction in an idealized setup. It focused on how geometry influences tensile strength, rather than on detailed fracture mechanisms or failure steps. While the model has

Table 3
Relevant material properties utilized for the FE analysis, taken from previous experiments on the same material at RT conditions.

Property	E_{11}/GPa	E_{22}/GPa	ν_{12}/-	ν_{23}/-	G_{12}/GPa
Measured value	158.8	6.9	0.3	0.3	5.2

* $E11$ and $E22$ represent the Young's modulus of the unidirectional laminate under tensile loads in the longitudinal and transverse directions, respectively. ν_{12} and ν_{23} are the corresponding Poisson's ratios, while G_{12} denotes the material's shear modulus.

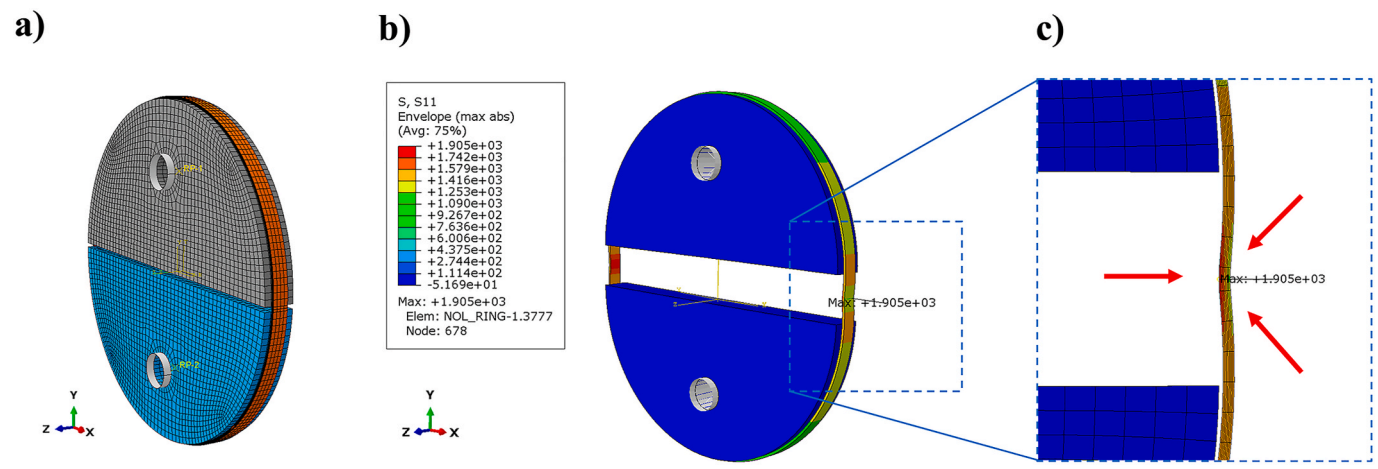

Fig. 10. a) FE mesh of the NOL-ring test setup, b) tensile failure for ¼″ NOL-ring specimen, c) approximated image of the NOL-ring specimen under tension.

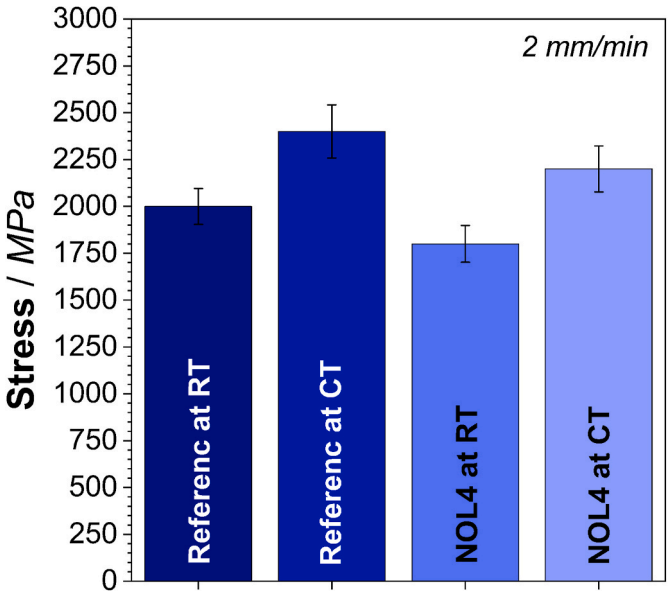

Fig. 11. Ultimate failure stress of reference tensile bars and NOL4 specimens at RT and CT.

limitations, particularly in capturing localized failure, it successfully correlates the observed strength decrease with changes in geometry, consistent with the experimental findings.

3.6. Tensile properties at cryogenics

The best-performing NOL-ring (NOL4) was additionally manufactured for testing in cryogenic environment. The autoclave flat tensile specimens served as a reference for these tests. Fig. 11 illustrates the tensile strength of the reference tensile bars and the NOL rings tested at 77 K, alongside the same systems tested at RT.

Both the tensile bars and NOL-ring specimens exhibited an increase in tensile strength when tested in cryogenic environment. This observation aligns with well-documented findings in the literature [29,30], which indicate the stiffening and shear-strengthening effect induced by the ultra-low temperature. At 77 K, the elastic modulus of the matrix increases significantly, compressing the fibers and enabling greater load transfer, as mentioned in Ref. [29]. However, the embrittlement effect at such low temperatures can reduce the failure strain, sometimes leading to lower strength values. Previous publications [30] reported increased sensitivity to defects and irregularities within the structure due to a reduction in the plastic zone radius at 77 K, ultimately affecting the material strength. The specifically designed for cryogenic environments matrix has a failure strain at 77 K (3.7 % [20]) still higher than the longitudinal strain failure of the fibers (1.8 %), allowing the longitudinal carbon-fibers to perform optimally. The tensile strength of the reference tensile bars increased notably from 2043 MPa to 2400 MPa, a rise of over 15 %. Similarly, the NOL4 system exhibited a significant increase from 1790 MPa to 2200 MPa, reflecting an improvement of more than 20 %. These comparable strength gains between tensile bars and the NOL-ring system highlight the stiffening effect resulting from the cryogenic environment.

The failure modes of the NOL-ring specimens differ significantly between RT and CT. At RT, the failure is characterized by longitudinal delamination, with most fibers remaining intact, indicating that shear failure is more pronounced than transversal microcracking of the matrix. This is reasonable as the cryogenic-design epoxy matrix has a high toughness and a lower elastic modulus, dissipating microcracks through the high plastic zone radius but decreasing the shear strength [30]. On the other hand, the increase in the modulus of the matrix caused by the ultra-low temperature environment could justify an increase in the shear strength and brittleness, being now more suceptibel to transversal microcracks. This would instead lead the composite material to fail suddenly rather than in a gradual manner, as shows Fig. 12. Interestingly, the reference tensile bar in cryogenic environments still follows a londitudinal delamination, probably expressing the full performance of the carbon-fibers and the possible decrease in failure strain of the matrix. However for the NOL-rings specimen, it is believed that the extra stress at the edge of the split-disk tool additional to the bending effect within the region, causes a decrease on the performance of the fibers, leading to a sudden transversal failure of the UD specimen. The failure here is located exactly at the region between the slipt-disks where the simulation analysis (Fig. 10c) indicates a bending effect. Despite the stress concentration in the tensile bars, the ultimate strength suggests that bending-induced stress in curved parts is far more critical than tab-induced stress in straight tensile bars. This highlights the influence of geometry on material performance under load.

4. Conclusions

In this study, CFRP NOL-ring specimens were manufactured using different winding processes to evaluate their effects on consolidation and layup regularity, and subsequently, their influence on the overall strength of the laminates. The key findings are summarized below:

Optical microscopy and profilometer analysis showed that external heating during winding is essential for achieving consolidation quality comparable to autoclave-cured laminates. Systems using heated slit-tape

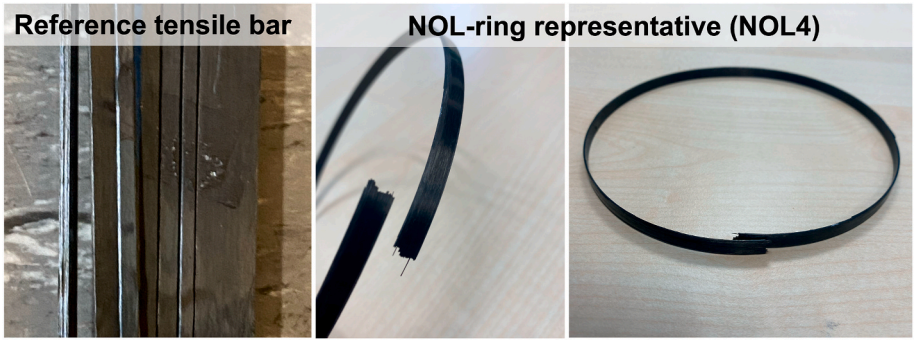

Fig. 12. Visual analysis of reference tensile bar and NOL-ring specimens tensile tested longitudinal to the carbon-fibers at 77 K.

and wet-wound towpregs demonstrated superior uniformity with minimal voids, unlike non-heated slit-tape systems, which exhibited significant irregularities and scattered defects. This is ultimately related to the resin state.

Resin viscosity and prepreg tack experiments revealed that a viscosity range of 10^4–10^6 mPa s promotes optimal consolidation and layup quality. Systems with resin that was too dry or too wet exhibited lower tack and poorer layup quality. Poor layup quality eventually resulted in reduced tensile strength of the material.

Systems with higher consolidation quality (NOL4, NOL5) achieved tensile strengths of 1790 MPa and 1828 MPa, closer to the autoclaved reference (2043 MPa). Poorly compacted specimens (NOL1, NOL2, NOL3) showed significantly lower tensile strengths (1430 MPa, 1570 MPa, and 1703 MPa). The geometric effect of transitioning from flat tensile bars to curved NOL-rings resulted in reduced tensile strengths due to pre-stress and curvature-induced bending. The NOL-ring specimen geometry introduces bending stresses that reduce the ultimate tensile strength compared to the reference specimens, exhibiting ultimate failure at 1900 MPa compared to the 2043 MPa of the reference specimen, even when ideal consolidation is assumed in FE analysis.

Finally, NOL-ring tensile testing was conducted at cryogenic temperatures (77 K), revealing substantial strength increases, as expected from the reference system. The NOL4 system improved from 1790 MPa at RT to 2200 MPa at CT (+23 %), while the reference tensile bar increased from 2043 MPa to 2400 MPa (+18 %). At CT, the resin stiffening facilitated better stress transfer to fibers, leading to higher strengths. NOL-ring specimens exhibited a transition from delamination at RT to fiber-dominated failure at cryogenics, while the autoclaved tensile bars failed similarly at both temperatures, showing longitudinal delamination towards the load.

This study highlights the importance of optimizing winding parameters and resin viscosity to improve the wound part performance. A thorough comparison of slit-tapes, towpregs, and winding parameters, with a novel focus on prepreg tackiness, demonstrate how properties can be maximized. Lastly, the novel approach for evaluating NOL-ring behavior in cryogenic environments provides valuable insights for applications such as cryogenic tanks.

CRediT authorship contribution statement

Eduardo Szpoganicz: Writing – review & editing, Writing – original draft, Visualization, Methodology, Investigation, Formal analysis, Data curation, Conceptualization. **Fabian Hübner:** Writing – review & editing, Validation, Supervision, Conceptualization. **Marius Luik:** Writing – review & editing, Validation, Investigation. **Jeremias Thomas:** Writing – review & editing, Validation, Investigation. **Florian Max:** Writing – review & editing, Validation, Investigation. **Andreas Scherer:** Writing – review & editing, Validation, Software, Formal analysis. **Tobias Dickhut:** Writing – review & editing, Validation. **Holger Ruckdäschel:** Writing – review & editing, Validation, Supervision.

Declaration of competing interest

The authors declare that they have no known competing financial interests or personal relationships that could have appeared to influence the work reported in this paper.

Acknowledgement

This project was carried out under the guidance of *Industrieanlagen-Betriebsgesellschaft mbH* (iABG) and financed by the Bavarian Ministry of Economic Affairs, Regional Development and Energy (STmWi) according to the registration number BLU-2109-0024. Moreover, we sincerely acknowledge Paul Mühlthaler for his assistance in testing the NOL-ring specimens in cryogenic environments.

Data availability

Data will be made available on request.

References

[1] R. Neugebauer, Hydrogen Technologies, Springer International Publishing, Germany, 2023.
[2] M. Yue, H. Lambert, E. Pahon, R. Roche, S. Jemei, D. Hissel, Hydrogen energy systems: a critical review of technologies, applications, Trends and challenges, Renew. Sustain. Energy Rev. 146 (2021) 111180, https://doi.org/10.1016/j.rser.2021.111180.
[3] M. Nachtane, M. Tarfaoui, M.A. Abichou, A. Vetcher, M. Rouway, A. Aâmir, H. Mouadili, H. Laaouidi, H. Naanani, An overview of the recent advances in composite materials and artificial intelligence for hydrogen storage vessels design, J. Compos. Sci. 7 (3) (2023) 119, https://doi.org/10.3390/jcs7030119.
[4] W. Gul, Y.E. Xia, P. Gérard, S.K. Ha, Characterization of polymeric composites for hydrogen tank, Polymers 15 (18) (2023) 3716, https://doi.org/10.3390/polym15183716.
[5] J. Zheng, X. Liu, P. Xu, P. Liu, Y. Zhao, J. Yang, Development of high pressure gaseous hydrogen storage technologies, Int. J. Hydrogen Energy 37 (1) (2012) 1048–1057, https://doi.org/10.1016/j.ijhydene.2011.02.125.
[6] J.B. Multhoff, J. Krieger, Effective structural design procedure for composite hydrogen tanks, in: Proc. 18th World Hydrogen Energy Conf., 2010. ISBN: 978-3-89336-654-5.
[7] W.-U. Herres, The hydrogen fuel cell vehicle – a future application for composites, in: Proc. Filament Winding Congress, 2005. Brussels.
[8] M.P. Alves, W. Gul, C.A. Ci Jr., S.K. Ha, A review on industrial perspectives and challenges on material, manufacturing, design and development of compressed hydrogen storage tanks for the transportation sector, Energies 15 (14) (2022) 5152, https://doi.org/10.3390/en15145152.
[9] M. Yang, R. Hunger, S. Berrettoni, B. Sprecher, B. Wang, A review of hydrogen storage and transport technologies, Clean Energy 7 (1) (2023) 190–216, https://doi.org/10.1093/ce/zkad021.
[10] M. Sippel, A. Kopp, D. Mattsson, S. Koussios, Advanced cryo-tanks structural design investigated in CHATT, in: *SSMET 2014*; Braunschweig, Germany, April 1–4, 2014. Available online: https://elib.dlr.de/89206/.
[11] H. Nojoumi, I. Dincer, G. Naterer, Greenhouse gas emissions assessment of hydrogen and kerosene-fueled aircraft propulsion, Int. J. Hydrogen Energy 34 (3) (2009) 1363–1369, https://doi.org/10.1016/j.ijhydene.2008.11.017.
[12] H.K. Rivers, J.G. Sikora, S.N. Sankaran, Detection of hydrogen leakage in a composite sandwich structure at cryogenic temperature, J. Spacecr. Rockets 39 (3) (2002), https://doi.org/10.2514/2.3829.
[13] K. Yonemoto, Y. Yamamoto, K. Okuyama, T. Ebina, Application of CFRP with high hydrogen gas barrier characteristics to fuel tanks of space transportation system,

Trans. JSASS Space Tech. Japan 7 (26) (2009) 13–18, https://doi.org/10.2322/tstj.7.Pc_13.
[14] M.T. Ahad, M.M.H. Bhulyan, A.N. Sakib, B. Corral, A. Siddique, An overview of challenges for the future of hydrogen, Materials 16 (20) (2023) 6680, https://doi.org/10.3390/ma16206680.
[15] T. Morimoto, T. Shimoda, Y. Morino, Y. Hayashi, T. Yokozeki, T. Ishikawa, Pressurizing test of CFRP model tank in cryogenic temperature, in: 10th AIAA/NAL-NASDA-ISAS Int. Space Planes Hypersonic Syst. Technol. Conf., American Institute of Aeronautics and Astronautics, Kyoto, Japan, 2001, https://doi.org/10.2514/6.2001-1882.
[16] X. Wang, T. Mingming, X. Chen, P. Xie, J. Yang, J. Chen, W. Yang, Advances on materials design and manufacture Technology of plastic liner of type IV hydrogen storage vessel, Int. J. Hydrogen Energy 47 (13) (2022) 8382–8408, https://doi.org/10.1016/j.ijhydene.2021.12.198.
[17] H.S. Roh, T.Q. Hua, R.K. Ahluwalia, Optimization of carbon fiber usage in type 4 hydrogen storage tanks for fuel cell automobiles, Int. J. Hydrogen Energy 38 (29) (2013) 12795–12802, https://doi.org/10.1016/j.ijhydene.2013.07.016.
[18] S.J. Canfer, D. Evans, Properties of materials for use in liquid hydrogen containment vessels, Adv. Cryog. Eng. Mater. 44 (1998) 1–10, https://doi.org/10.1007/978-1-4757-9056-6_34.
[19] M. Azeem, H.H. Ya, M.A. Alam, M. Kumar, P. Stabla, M. Smolnicki, L. Gemi, Application of filament winding Technology in composite pressure vessels and challenges: a review, J. Energy Storage 49 (2022) 103468, https://doi.org/10.1016/j.est.2021.103468.
[20] F. Hübner, A. Brückner, T. Dickhut, V. Altstädt, A.R. De Anda, H. Ruckdäschel, Low temperature fatigue crack propagation in toughened epoxy resins aimed for filament winding of type V composite pressure vessels, Polym. Test. 102 (2021) 107323, https://doi.org/10.1016/j.polymertesting.2021.107323.
[21] K.C. Jois, T. Mölling, T. Gries, J. Sackmann, Towpreg-based design and manufacture of multi-supply filament-wound composite pressure vessels, in: *SAMPE neXus Proceedings*; Society for the Advancement of Material and Process Engineering, North America, July 2021.
[22] S. Sihn, R. Kim, K. Kawabe, S. Tsai, Experimental studies of thin-ply laminated composites, Compos. Sci. Technol. 67 (6) (2007) 996–1008, https://doi.org/10.1016/j.compscitech.2006.06.008.
[23] A. Beakou, M. Cano, J.B. Le Cam, V. Verney, Modelling slit tape buckling during automated prepreg manufacturing: a local approach, Compos. Struct. 93 (10) (2011) 2628–2635, https://doi.org/10.1016/j.compstruct.2011.04.030.
[24] C. Schillo, D. Röstermundt, D. Krause, Experimental and numerical study on the influence of imperfections on the buckling load of unstiffened CFRP shells, Compos. Struct. 131 (2015) 128–138, https://doi.org/10.1016/j.compstruct.2015.04.032.
[25] F. Schönl, F. Hübner, M. Luik, J. Thomas, R. Albuquerque, H. Ruckdäschel, Digital approaches for optimization of composite processing: bayesian optimization for impregnation and fibre spreading in-situ monitoring. Proceedings of the Munich Symposium on Lightweight Design 2022, Springer Vieweg, Cham, 2022, https://doi.org/10.1007/978-3-031-33758-1_5.
[26] E. Szpoganicz, M. Demleitner, F. Hübner, Y. Oh, Y. Kweon, H. Lee, V. Altstädt, H. Ruckdäschel, Phenolic prepregs for automated composites manufacturing – correlation of rheological properties and environmental factors with prepreg tack, Compos. Sci. Technol. 218 (2022) 109188, https://doi.org/10.1016/j.compscitech.2021.109188.
[27] A.R. Ghasemi, M. Moradi, Failure analysis of the nol-ring polymer matrix composites under thermal cycling, Polym. Compos. 39 (9) (2018) 3140–3146, https://doi.org/10.1002/pc.24320.
[28] Z. Jiao, Z. Yao, J. Zhou, P. Yi, C. Lu, Reinforced interface and mechanical properties of high strength carbon fiber composites, High Perform. Polym. 32 (5) (2020) 663–673, https://doi.org/10.1177/0954008320957398.
[29] Z. Sápi, R. Butler, Properties of cryogenic and low temperature composite materials – a review, Cryogenics 111 (2020) 103190, https://doi.org/10.1016/j.cryogenics.2020.103190.
[30] E. Szpoganicz, F. Hübner, U. Beier, M. Geistbeck, H. Ruckdäschel, The effect of prepreg ply thickness in carbon fiber reinforced composites on intralaminar toughness and shear strength in cryogenic environments for liquid hydrogen storage tanks, Composites, Part B 253 (2024), https://doi.org/10.1016/j.compositesb.2024.112077.